韓國水資源學會論文集
第38卷 第5號 · 2005年 5月
pp. 365~377

수력터빈 드래프트관을 통과하는 물고기에 미치는 난류의 영향 수치모의

Numerical Investgation of the Effect of Turbulent Flow on Fish Passing through Hydroturbine Draft Tube

백 중 철*
Paik, Joongcheol

Abstract

This paper presents numerical works carried out for developing an advanced computational framework for understanding injury- and mortality-inducing flow phenomena in hydropower facilities. Large-eddy simulation (LES) of a circular jet flow is carried out to help interpret the results of recent experiments that exposed live fish to the shear zone of a turbulent jet. The instantaneous flow field of LES is characterized by intense velocity, pressure, and vorticity fluctuations, which could exert forces and moments on a fish considerably larger than those exerted by the same fish exposed to the corresponding steady, time-averaged flow. In this study, also, unsteady modeling of flow in a hydroturbine draft tubewas carried out using a hybrid unsteady RANS/LES, so-called detached-eddy simulation (DES). Results from DES show that the potential for disorientation and excessive residence times of fish within the draft tube is certainly considerable.

keywords : Numerical simulation, Fish, Turbulent flow, Hydroturbine draft tube

요 지

본 연구는 수력발전시설에서 물고기의 생존과 상해를 유도하는 흐름현상을 파악하기 위한 진보된 수치해석기법의 개발을 다루고 있다. 원형 젯의 LES를 실시하여 난류젯의 전단지역에 물고기를 방류하는 실험의 결과를 수치적으로 해석하였다. 이 연구에서는 순간 LES 흐름장이 유속, 압력 그리고 와도의 강한 변동으로 특성지울 수 있으며, 이것이 물고기에게 시간평균 정상류보다 상당히 큰 추진력과 모멘트를 발휘함을 보여준다. 이 연구는 아울러 수력터빈 드래프트관에서의 부정류를 RANS/LES의 혼성모형 즉 DES를 이용하여 해석하였으며, 물고기가 드래프트관내에서 방향감각을 상실하거나 과도하게 지체하도록 할 수 있는 난류가 발생함을 보여준다.

핵심용어 : 수치모의, 물고기, 난류, 수력터빈 드래프트관

1. Introduction

Today, the hydropower industry is confronted with the challenging task of improving the environmental compatibility of its facilities. A pressing environmental concern is the potentially adverse impact on fish that pass through the hydropower plant, which could be detrimental to the populations of migrating fish species like salmon. Fish injuries and even mortality are known to occur

* 조지아공대 토목환경공학과, 연구원
Research Engineer, School of Civil and Environmental Engineering, Georgia Institute of Technology, Atlanta, Georgia 30332-0355 USA.
(e-mail: joongcheol.paik@ce.gatech.edu)

as a result of the interaction of fish with the solid structures within the hydropower plant and the complex flow characteristics these structures induce. A major goal of this study is to provide basic scientific knowledge tohelp minimize the potential for disorientation,injury and mortality of fish passing through hydropower facilities. Fish passage through hydropower facilities, however, is a difficult problem to study because little is known about the biological effect and relative importance of various flow-induced forces (due to shear, turbulence, rapid pressure changes, cavitation, etc.) on fish. The behavior of individual fish and fish species as it relates to fish passage is also a complicating factor that must be understood and taken into account (Coutant and Whitney 2000). Recent laboratory experiments with live fish have attempted to isolate and explore separately some of these effects (Nietzel *et al.* 2000; Abernethy *et al.* 2001). Such experiments have enhanced overall understanding of fish/flow interaction, but by themselves these experiments can neither reproduce nor elucidate the real flow environment experienced by fish passing through a hydropower installation. The geometrical complexity of a typical hydropower installation along with the rotation of the turbine runner induce a very complex flow environment that is characterized by highly unsteady, large-scale vortices; regions of intense turbulence production; pockets of high shear; regions of flow reversalcollapsing cavitation bubbles; etc. Fish trajectories in such a complex flow environment are chaotic and the histories of various flow-induced forces experienced by a passing fish are very hard, if not impossible, to quantify experimentally. In fact, even simple measurements of basic flow quantities within a hydropower facility are difficult to obtain because most parts of the facility are enclosed and cannot be readily accessed.

All of these considerations make it apparent that computational fluid dynamics (CFD) modeling of the unsteady flow within the hydropower plant as well as its impact on passing fish is a critical prerequisite for understanding fish passage and for improving the fish friendliness of hydropower facilities. This paper is aimed at developing the computational infra-structure for simulating fish passage through hydropower plants. This study has a two-pronged approach: (1) unsteady CFD modeling of recently conducted laboratory experiments with live fish in relatively simple turbulent flows (Neitzel *et al.* 2000) to help interpret the results of these experiments and facilitate the design of future, more-focused laboratory studies; and (2) unsteady CFD modeling of flow in various components of a hydropower facility to understand the real-life flow environment experienced by passing fish.

In CFD, there are presently two modeling extremes for the prediction of turbulent flows. At one extreme is direct numerical simulation (DNS) and its close cousin LES. Although they are the most scientifically rigorous, both of these modeling approaches become prohibitively expensive for wall-bounded flows at high Reynolds numbers. Unfortunately, hydropower facilities contain a multitude of walls and the flow through them occurs at very high Reynolds numbers. At the other extreme of turbulence modeling is the so-called Reynolds-average Navier - Stokes (RANS) approach where time-averaging is used to transform the instantaneous equations of mass and momentum conservation into equations for the statistical mean flow quantities (mean velocity components and pressure). Although much cheaper computationally, traditional RANS methods only predict the steady mean flow, and therefore, by themselves cannot provide the unsteady component of the flow that is necessary to accurately calculate the trajectories of fish through hydropower facilities and thus predict the unsteady forces of the fluid on the fish. Spalart (2000) presents a good discussion of these different approaches to unsteady turbulence modeling in the context of the aerospace industry. Paik *et al.* (2005) discussed these same approaches for internal hydro-dynamic applications. An approach for predicting high Reynolds number flows that are too expensive to compute with DNS or LES even with the current generation of supercomputers is the so-called detached-eddy simulation (DES) (Spalart 2000). The DES technique combines an unsteady version of RANS near the walls with a version of LES in regions of the flow where most of the turbulence can

be captured inexpensively (that is, on computational grids that are not too dense).

This study first present some recent LESthat was performed in support a laboratory study of the effects of shear and turbulence on fish in a turbulent jet (Nietzel *et al.* 2000). This study also developed a particle-tracking module that predicts the trajectories of fluid (massless) particles or fish-like particles both in an unsteady manner. PresentCFD model of the jet underscores the importance of accounting for the inherent unsteady nature of turbulent flows when trying to understand the effects of a turbulent flow on fish. Subsequently, this paper briefly summarizes some results from DESproviding affordable, yet accurate, unsteady turbulent flow in a hydroturbine draft tube.

2. Governing Equation

2.1 The Mean Flow Equations

The governing equations for the mean flow are the three-dimensional, unsteady, incompressible, Reynolds-averaged Navier-Stokes (RANS) equations. By invoking the Boussinesq hypothesis to express the Reynolds stresses in terms of the mean rate of strain tensor, the governing equations can be written in strong-conservation form in generalized, curvilinear coordinates as follows,

$$\Gamma\frac{\partial Q}{\partial t}+J\frac{\partial}{\partial \xi^j}\left(F^j-F_v^j\right)=0 \tag{1}$$

where

$$\Gamma=\mathrm{diag}[0,\ 1,\ 1,\ 1] \tag{2}$$

$$Q=[P,\ u_1,\ u_2,\ u_3]^T \tag{3}$$

$$F_f^j=\frac{1}{J}\left[\beta U^j,\ u_1U^j+p\xi_{x_1}^j,\ u_2U^j+p\xi_{x_2}^j,\ u_3U^j+p\xi_{x_3}^j\right]^T \tag{4}$$

$$F_v^j=\frac{1}{J}\left(\nu_t+\frac{1}{\mathrm{Re}}\right)\left[0,\ g^{mj}\frac{\partial u_1}{\partial \xi^m},\ g^{mj}\frac{\partial u_2}{\partial \xi^m},\ g^{mj}\frac{\partial u_3}{\partial \xi^m}\right]^T \tag{5}$$

In the equations above, the term P is a modified pressure $P=p/\rho+2k/3$ where p is the piezometric pressure and k is the turbulent kinetic energy, $u_i(i=1,2,3)$ are the Cartesian velocity components, x_i are the Cartesian coordinates, J is the Jacobian of the geometric transformation, ζ_{xj}^i are the metrics of the geometric transformation, U^j are the contra-variant velocity components $U^j=u_i\zeta_{xj}^i$, g^{ij} are the components of the contravariant metric tensor $g^{ij}=\xi_{x_k}^i\xi_{x_k}^i$, Re is the Reynolds number, and ν_t is the turbulent viscosity.

2.2 The LES model

In LES, only turbulent eddies larger than the grid size are directly computed while the effect of smaller eddies (so-called subgrid eddies) is models. To separate the large eddies from the small eddies, the three-dimensional, instantaneous Navier-Stokes equations are filtered in space. This spatial filtering operation is designed to remove from the equations scales of motion whose size is smaller than the filter width. The resulting spatially filtered equations look exactly like the Navier-Stokes equations for the spatially averaged velocity pressure fields plus an additional subgrid term, which represents the effects of the small eddies on the resolved flow.

Many different subgrid-stress (SGS) models have been proposed in the literature with varying levels of complexity and associated computational cost. In fact, some LES studies of free shear flows use on explicit turbulence model and rely instead on the dissipation inherent in the numerical scheme to suppress the small, unresolved scales of turbulence (Grinstein and Devore, 1996). The standard Smagorinsky (1963) SGS model is used in this study, which was successfully used in a recent LES study of turbulent flows in rectangular jets by Wilson and Demuren (1998). The Smagorinsky model is a simple, algebraic model based on the eddy viscosity concept

$$\tau_{ij}=\frac{1}{3}\delta_{ij}\tau_{kk}-2\nu_tS_{ij} \tag{6}$$

where δ_{ij} is the Kronecker's delta. This Eq. (6)

relates the subgrid-scale stresses τ_{ij} to the large-scale strain-rate tensor S_{ij} and is calculated

$$S_{ij} = \frac{1}{2}\left(\frac{\partial u_i}{\partial x_j} + \frac{\partial u_j}{\partial x_i}\right) \tag{7}$$

In the Smagorinsky model, the eddy viscosity is calculated as

$$\nu_t = C\Delta^2|S| \tag{8}$$

where C is a constant set equal to 0.01 - a value typically used for shear flows (Wilson and Demuren, 1998). For the anisotropic grid used in this study, the grid size Δ is computed at each grid point as

$$\Delta = (\Delta_1\Delta_2\Delta_3)^{\frac{1}{3}} \tag{9}$$

The magnitude of the strain-rate tensor is

$$|S| = (2S_{ij}S_{ij})^{\frac{1}{2}} \tag{10}$$

2.3 The DES model

Detached-eddy simulation (DES) was proposed by Spalart *et al.* (1997) and is based on the Spalart-Allmaras (S-A) one-equation turbulence model (Spalart-Allmaras, 1994).

$$\frac{\partial \tilde{\nu}}{\partial t} + J\frac{\partial}{\partial \xi^m}\left[\frac{1}{J}\left(U^j\tilde{\nu} - \frac{1}{\sigma}\left(\frac{1}{\mathrm{Re}} + \tilde{\nu}\right)g^{mj}\frac{\partial \tilde{\nu}}{\partial \xi^m}\right)\right] + JH_t = 0 \tag{11}$$

where

$$H_t = -c_{b1}\tilde{W}\tilde{\nu} + c_{w1}f_w\left(\frac{\tilde{\nu}}{\lambda}\right)^2 - \frac{1}{\sigma}c_{b2}\frac{\partial \tilde{\nu}}{\partial \xi^m}\frac{\partial \tilde{\nu}}{\partial \xi^m} \tag{12}$$

The turbulent viscosity ν_t is linked to the working variable $\tilde{\nu}$ and a wall function f_{v1} by

$$\nu_t = \tilde{\nu}f_{v1}, \quad f_{v1} = \frac{\chi^3}{\chi^3 + c_{\mu 1}^3}, \quad \chi = \frac{\tilde{\nu}}{\nu} \tag{13}$$

where ν is the molecular viscosity. The modified vorticity $\tilde{W}$ is defined in terms of the magnitude of the vorticity W as,

$$\tilde{W} = f_{\mu 3}W + \frac{\tilde{\nu}}{\kappa^2\lambda^2}f_{v2}, \quad f_{v2} = \left(1 + \frac{\chi}{c_{v2}}\right)^{-3}, \quad f_{v3} = \frac{(1+\chi f_{v1})(1-f_{v2})}{\chi} \tag{14}$$

where λ is the distance to the nearest wall. The production term as written in Eq. (14) differs from that developed in Spalart and Allmaras (1994) via the introduction of f_{v3} and re-definition of f_{v2}. These changes do not alter predictions of fully turbulent flows and have the advantage that for simulation of flows with laminar separation, spurious upstream propagation of the eddy viscosity into attached, laminar regions is prevented (Squires et al. 2002). The wall destruction function f_w is given by

$$f_w = g\left[\frac{1+c_{w3}^6}{g^6 + c_{w3}^6}\right], \quad g = r + c_{w2}(r^6 - r), \quad r \equiv \frac{\tilde{\nu}}{\tilde{W}\kappa^2 d^2} \tag{15}$$

The closure coefficients are,

$$c_{b1} = 0.1355, \quad \sigma = 2/3, \quad c_{b2} = 0.622$$

$$\kappa = 0.41, \quad c_{w1} = \frac{c_{b1}}{\kappa^2} + \frac{(1+c_{b2})}{\sigma}, \quad c_{w2} = 0.3 \tag{16}$$

$$c_{w3} = 2, \quad c_{v1} = 7.1$$

The DES formulation is obtained by replacing the distance to the nearest wall λ in the S-A model by the modified length scale $\tilde{\lambda}$ defined as

$$\tilde{\lambda} \equiv \min(\lambda, C_{DES}\Delta) \tag{17}$$

where the model constant C_{DES} = 0.65 was set in homogeneous turbulence (Shur *et al.* 1999). Assuming that the computational mesh is constructed such that the wall-parallel grid spacing is of the order of the boundary layer thickness, the S-A unsteady RANS

model is retained throughout the boundary layer, i.e., $\tilde{\lambda}=\lambda$. Consequently, prediction of boundary layer separation is determined in the URANS mode of DES. Far from the solid boundaries, the model becomes a one-equation model for the sub-grid scale (SGS) eddy viscosity. When the production and destruction terms of the model are balanced, the length scale $\tilde{\lambda}= C_{DES}\Delta$ in the LES region yields a Smagorinsky eddy viscosity $\tilde{\nu} \propto S\Delta^2$. Analogous to classical LES, the role of Δ is to allow the energy cascade down to the grid size; roughly, it makes the pseudo-Kolmogorov length scale, based on the eddy viscosity, proportional to the grid spacing.

3. Numerical Methods

The 3D, incompressible, URANS and turbulence closure equations formulated in generalized, curvilinear coordinates in strong conservation form are solved using a dual-time-stepping artificial compressibility (AC) iteration scheme. Due to space considerations, a brief description of the numerical methods is given in this paper (see Paik *et al.,* 2005 for details). The AC forms of the governing equations are discretized using a second-order-accurate finite-volume method on a non-staggered computational grid. The convective terms are discretized using the QUICK scheme, and central differencing is employed for the pressure gradients, viscous fluxes and source terms in the turbulence equation. The third-order artificial dissipation method of Sotiropoulos and Adballah (1992) is employed for pressure to eliminate odd-even decoupling of the pressure field. The physical time derivatives are discretized with three-point-backward, Euler-implicit temporal-integration scheme. The discrete equations are marched in time to advance the solution to the next time step by adopting the dual- (or pseudo-) time-stepping method which needs to be integrated in pseudo-time until the pseudo-time derivative is reduced to a prescribed small tolerance and the governing equations are satisfied at the advanced time level. The system of equations are integrated in pseudo time using the pressure-based implicit preconditioner of Sotiropoulos and Constantinescu (1997) enhanced with local-time-stepping and V-cycle multigrid acceleration.

The turbulencestatistics of the flow should not be compromised by the extension of the computational domain and/or the outlet boundary conditions. The characteristics-based, non-reflecting boundary conditions developed by (Paik *et al.* 2005) in the frame of the pressure-based implicit preconditioner is applied at the outlet to allow statistically complete vortical structures to exit the computational domain. The domain-decomposition approach with structured, overset (Chimera) grids is employed for discretizing multi-connected geometry. The overset grid method in conjunction with robust pressure-based approximate factorization method employed in this work was found to allow efficient and stable unsteady simulations without non-physical spurious oscillationin the overlap region. The non-reflecting boundary condition also appeared to specify outflow boundary conditions without distorting the complex physics of the flow (see Paik *et al.,* 2004).

4. Results and Discussion

4.1 Modeling Studies of the Effects of Turbulence on Fish

Data from experiments of Nietzel *et al.* (2000) for several species of fish exposed to a submerged jet issuing into a stagnant reservoir were used to estimate "no-effect" thresholds from shear-induced fluid forces. In the laboratory experiments, turbulence-induced effects were observed by video taping the trajectories of the fish in the turbulent jet. These videos show that each fish underwent complex bending and flexing motions as it moved through the jet. Moreover, these motions varied widely from trial to trial with no two trials being exactly alike. These variations are consistent with the chaotic and unsteady nature of turbulent flows (Nietzel *et al.,* 2000).

In part to study these turbulence-induced variations, this study carried out LES to reproduce the turbulent and also developed a particle-tracking

module that predicts the trajectories of fluid (massless) particles or fish-like particles both in an unsteady manner. Figure 1 illustrates the computational domain used for these simulations and shows the location of the fish injection for the experiments and the computations. The extent of the jet within the computational domain is illustrated in Figure 1 by an isosurface of mean axial velocity. Figure 1 also shows the coordinate system that is used in the rest of this section. The x coordinate is oriented along the axis of the jet with the velocity component in this direction called u. The y and z coordinates are oriented in the transverse directions with the velocity components in those directions called v and w, respectively. For the model, this studyignored the fish-injection tube that was present in the experiments because including it would have significantly increased the computational cost of the simulation.

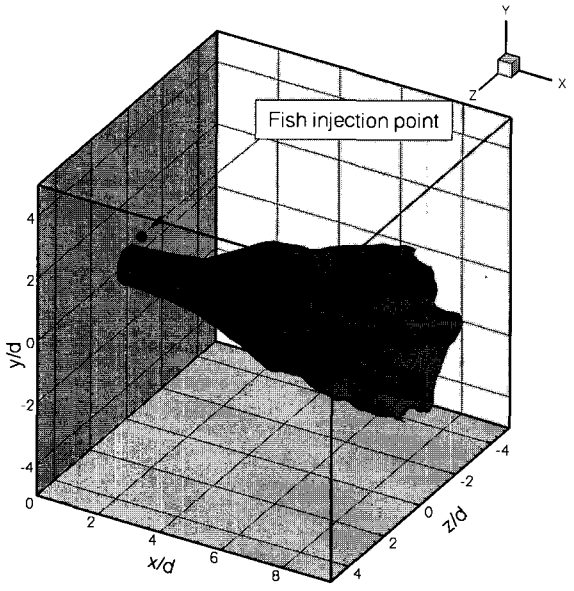

Fig. 1. Three-dimensional picture of the jet simulation with an isosurface of mean axial velocity showing the extent of the jet.

To see how well the computations reproduced the experiments, extensive comparisons were performed for Reynolds numbers of 100,000 and 300,000 both of which were used in the experiments. The Reynolds number is calculated as $u_j \mathrm{d}/\nu$ where u_j is the mean jet velocity, d is the diameter of the jet, and ν is the kinematic viscosity of the water. The Reynolds number is a measure of the ratio of the inertial forces to the viscous forces in a flow. In general terms, high Reynolds numbers indicate whether or not a flow is turbulent. The Reynolds numbers in these studies are well into the fully turbulent region for jets.

Figure 2 compares the mean-axial-velocity profiles in the experiments, measured using laser Doppler velocimetry (Nietzel *et al.* 2000), and the mean profiles from the simulations for a Reynolds number of 100,000. The mean for the simulation was computed from 160 equally spaced realizations out of a total 4000 time steps. Profiles of the mean axial velocity (u) are shown as a function of the vertical distance (y) away from the center of the jet. Overall, the computed mean-axial-velocity profiles are in excellent agreement with the measurements. Some small discrepancies occurred between $1\mathrm{d} < x < 2\mathrm{d}$, where the experimental profiles spread faster that in the simulation. However at x = 5d, the predictions and the experiments practically coincide. These discrepancies are likely due to the presence of the fish-injection tube in the experiment and its absence from the simulation. The shedding of vortices from the surface of the fish-injection tube would likely increase the level of turbulent mixing thus causing the jet to spread faster. Although to conserve space this paper doesn't show it here, the model predictions of the turbulence statistics also agree with the experiments especially in the region x > 5d where differences in initial conditions between the simulations and the experiments have little effect.

Comparisons of individual realizations of the simulated jet give a good sense of how widely the jet changes in time. Figure 3 shows instantaneous profiles of the axial velocity with the mean velocity profile superimposed on them as a thick black line for three locations downstream of the jet. These profiles show that the variation of the velocity is large especially outside the core of the jet in the so-called shear layer. In the shear layer, the velocities vary by as much as ±50% from the mean value. However, the fluid velocity is not the best quantity for representing the effect of the flow on the fish. From the perspective of a fish, the gradients of

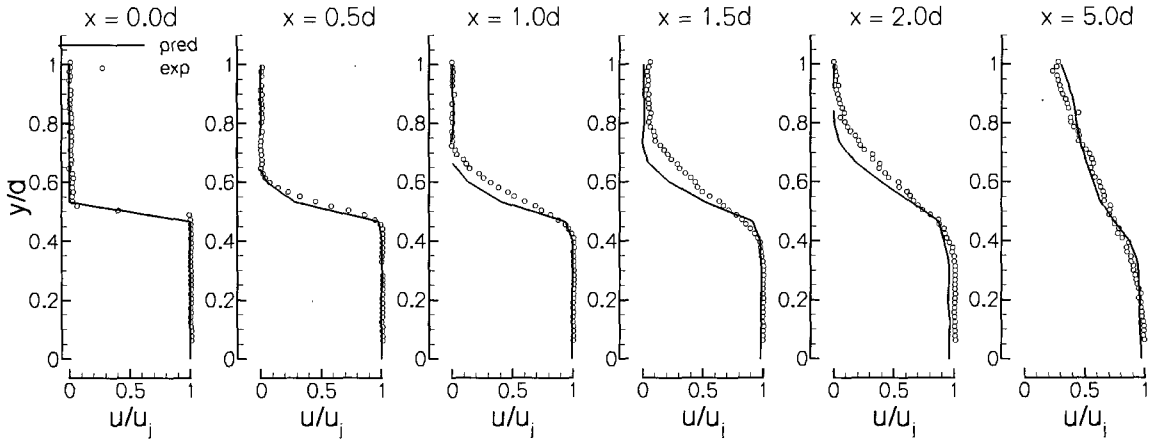

Fig. 2. Comparison of the mean-axial-velocity profile in the experimental (circles) and simulated (lines) jet for several locations downstream of the jet nozzle.

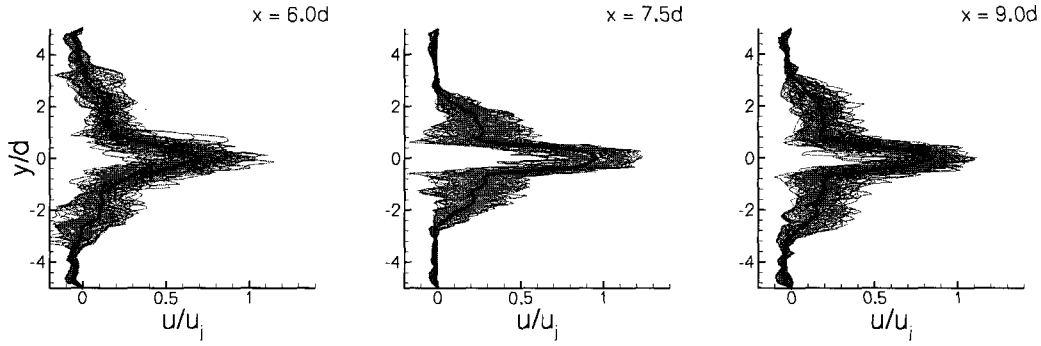

Fig. 3. Instantaneous profiles of the axial velocity (thin, gray lines) compared to the mean profile (thick, black line) at three locations downstream of the jet nozzle.

the velocity are more representative because fluid stresses are computed from velocity gradients, that is, the rate at which the velocity changes over distance.Therefore, at the same locations downstream of the jet nozzle, Figure 4 shows instantaneous profiles of the total vorticity with the mean vorticity superimposed on them. The total vorticity (which is computed from velocity gradients) is a measure of therotation that occurs at that point in the flow. In simple terms, the vorticity can be used to obtain estimates of the bending, flexing, and spinning torque that the fluid exerts on a fish. The vorticity profiles shown in Figure 4 are similar to the velocity profiles in Figure 3, but significant quantitative differences are evident. The intensity of the vorticity fluctuations about the mean is significantly higher than the fluctuations of the axial velocity component throughout the jet. In fact, there are several instantaneous profiles where the vorticity magnitude is almost an order of magnitude larger than the mean value. To reinforce the differences between the instantaneous and mean flow fields, Figure 5 compares the two using a three-dimensional picture of the flow. Figure 5(a) shows a snapshot of an isosurface of constant vorticity magnitude for an instantaneous flow field, and Figure 5(b) shows the same isosurface for the time-averaged mean flow. Obviously, the instantaneous flow field contains a much more complex structure. The range of scales that is typical of turbulent flows can also be observed in Figure 5(a) with some very small structures—much smaller than the diameter of the jet—appearing alongside structures that appear to be one or twodiameters long. On the other hand, the mean flow contains none of this complexity and little variation along the entire length of the jet. In summary,

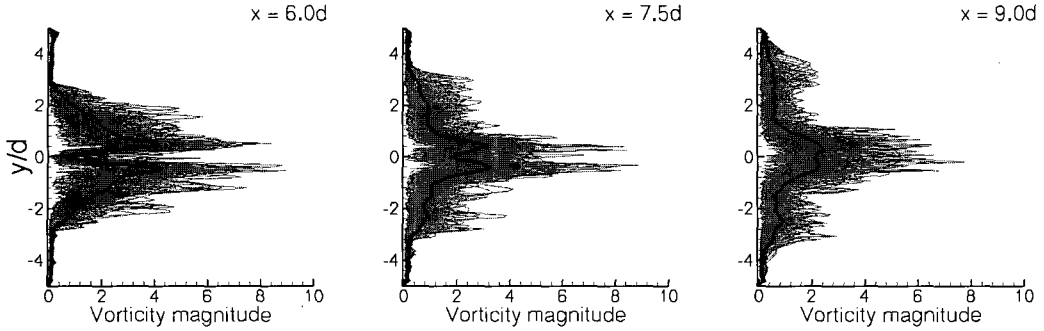

Fig. 4. Instantaneous profiles of the vorticity magnitude (thin, gray lines) compared to the mean profile (thick, black line) at three locations downstream of the jet nozzle.

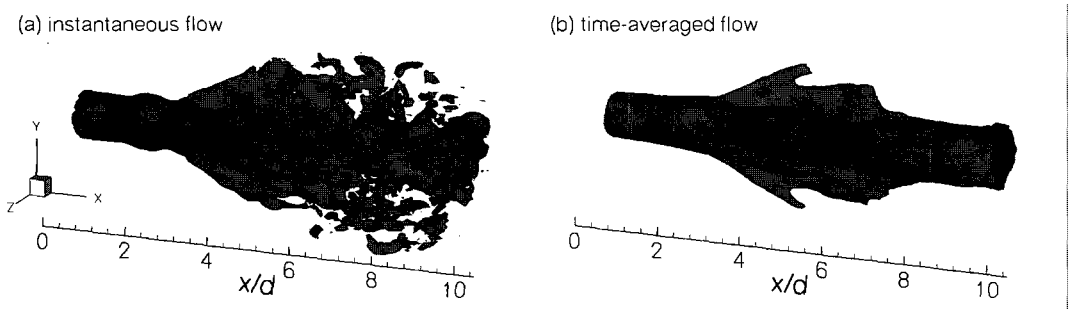

Fig. 5. Three-dimensional structure of the jet shown using an isosurface of the vorticity magnitude for the (a) instantaneous and (b) time-average flow.

Figures 3-5 clearly indicate that the instantaneous flow and not the mean flow must be considered for a meaningful interpretation of the injury, disorientation, mortality of fish exposed to a turbulent flow. Clearly the flow environment encountered by the fish is far more complicated and could be considerably more (or less) hazardous than mean flow measurements alone would suggest.

To further investigate the variation of individual fish trajectories, this studyused an existing virtual-fish model (Sotiropoulos and Ventikos 1997) that was developed to track fish-like objects in a steady flow field. The present virtual-fish model represents the fish as a rigid object shaped like a prolate spheroid to approximate the generic shape of a fish. At each time step, the fluid forces exerted on the virtual fish are computed and the equations of motion for the fish are integrated in time. A total of six equations are used to describe the entire spectrum of translations and rotations of the virtual fish in a three-dimensional flow. Calculated instantaneous snapshots of the locations of the fish in the flow are shown in Figure 6. This figure reveals the complex range of motions that the virtual fish undergoes in the instantaneous flow field. The

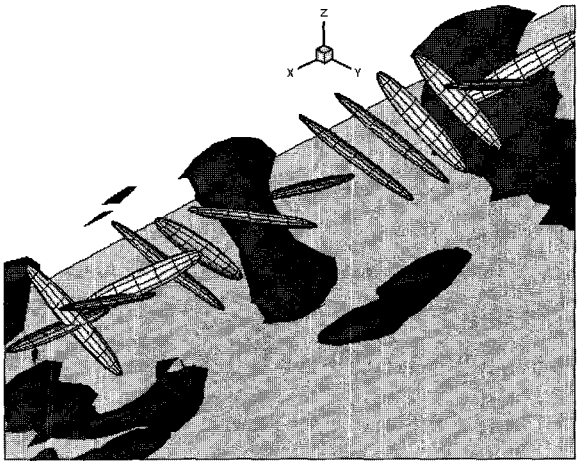

Fig. 6. Instantaneous snapshots of the location and orientation of the virtual fish in the instantaneous flow field of the jet. Isosurfaces (dark gray) of the vorticity magnitude of the jet at one instant in time are show for reference.

instantaneous shear magnitude on the fish was recorded at all points on the body of the fish for each time step. Like the vorticity magnitude in Figures 4 and 5, the shear magnitude is computed from the gradients of the velocity field and is related to the instantaneous shearing forces that the fluid exerts on the fish. Figure 7 shows a side-by-side comparison of the shear magnitude on a fish placed in the unsteady flow field with a fish released at the same location but using the mean jet flow field. The fish in the unsteady flow field experiences higher strain magnitudes as it passes through the jet. Moreover, at least three times this particular fish experiences instantaneous shear magnitudes that are more than twice as high as any of the shear magnitudes experienced by the fish in the steady flow. These extreme values are the ones that would be expectedto kill or injure a fish. Note also that the trajectories of these two virtual fish through the jet are different. In fact, fish released into the unsteady flow from the same location but at different times will have different

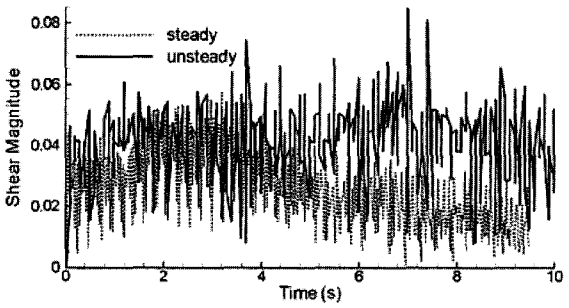

Fig. 7. Time history of the shear magnitude for the virtual fish in the steady and the unsteady flow fields.

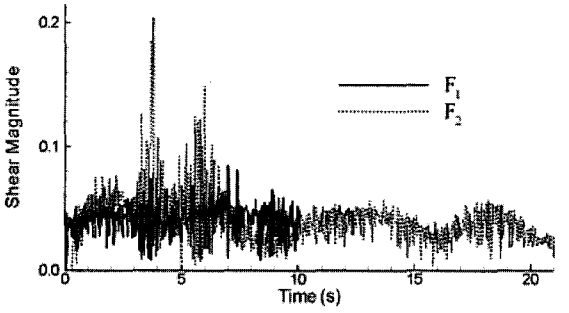

Fig. 8. Time history of the shear magnitude for the F_1 (virtual fish release in the unsteady flow) and F_2 (another virtual fish released 0.3 seconds later).

trajectories and experience significantly different shear magnitudes. Figure 8 shows a side-by-side comparison of the shear magnitudes experienced by two fish released into the unsteady flow separated only by 0.3 seconds. The fish F_1 in Figure 8 exits the computational domain in half the time it takes for the fish F_2. So the fish obviously take different trajectories though the jet even though they were released at the same point in the flow. Moreover, the fish F_2 experiences shear magnitudes two and three times larger than any of the shear magnitudes experienced by the fish F_1 in Figure 8.

4.2 Unsteady Turbulence Modeling of Hydropower Installations

In this section, recent progress toward computing the flow within in a draft tube using the DES technique is discussed. This work has begun to use the code to predict the flow in a scale model of the Norris draft tube of the Tennessee Valley Authority. The scale model was designed and studied by Hopping (1992) and was the subject of earlier steady RANS simulations (Ventikos *et al.* 1996). Using a multiple, arbitrarily overlapping computational grid containing approximately 10^6 nodes (see Figure 9 for a three-dimensional view of the multi-block computational mesh), several thousand time steps are predicted at a Reynolds number of 10^6.

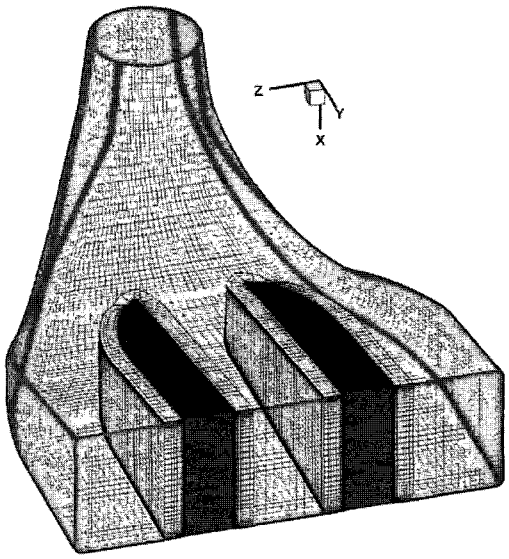

Fig. 9. Computational mesh of the draft tube showing the overlapping multiple grid blocks that are used to define the piers.

The draft tube takes the flow from the turbine and through a bend redirects into the river. The flow after the bend is divided into three bays by two piers. Figure 10 shows snapshots of the cross-stream velocity vectors in the three sections at three instants intime. The velocity vectors clearly show how complex the instantaneous flow is in this region and demonstrate how varied the flow can be from one instant in time to the next. It should be noted that the velocity profile used to specify inflow conditions at the draft-tube inlet accounts for the swirling flow that enters the draft-tube from the runner. Figure 11 shows instantaneous particle traces in the draft tube at the three instants in time. These particles are massless fluid particles and not the fish-like objects used in the previous section for the jet simulations. The particle paths in Figure 11 indicate the highly three-dimensional state of the flow field and give an indication of the variety of trajectories that a fish could take within the draft tube. Note that at one instant in time, Figure 11(c), no particles enter the center bay of the draft tube.

Figure 12 gives a snapshot of just a few instantaneous particle traces at a one instant in time. A couple of the particle paths enter the middle section only to be forced out of that section and into the right section where they exit the draft tube. Another trajectory in the middle section gets caught in a recirculating eddy. This study highlights the particle trajectories shown in this figure because there have been anecdotal reports of similar behaviors for nearly massless beads in the scale models of draft tubes. Furthermore, there is a growing awareness among the hydropower and fisheries communities that indirect mortality due to excessive disorientation of fish downstream of the turbine runner (that is, in the draft tube and the tailrace) may account for a significantly greater percentage of the total mortality within the hydropower plant than previously believed. Flow-induced disorientation, although not directly lethal, can significantly impair the ability of fish exposed to the turbine flow to escape from downstream awaiting predators, thus, making them easy pray.

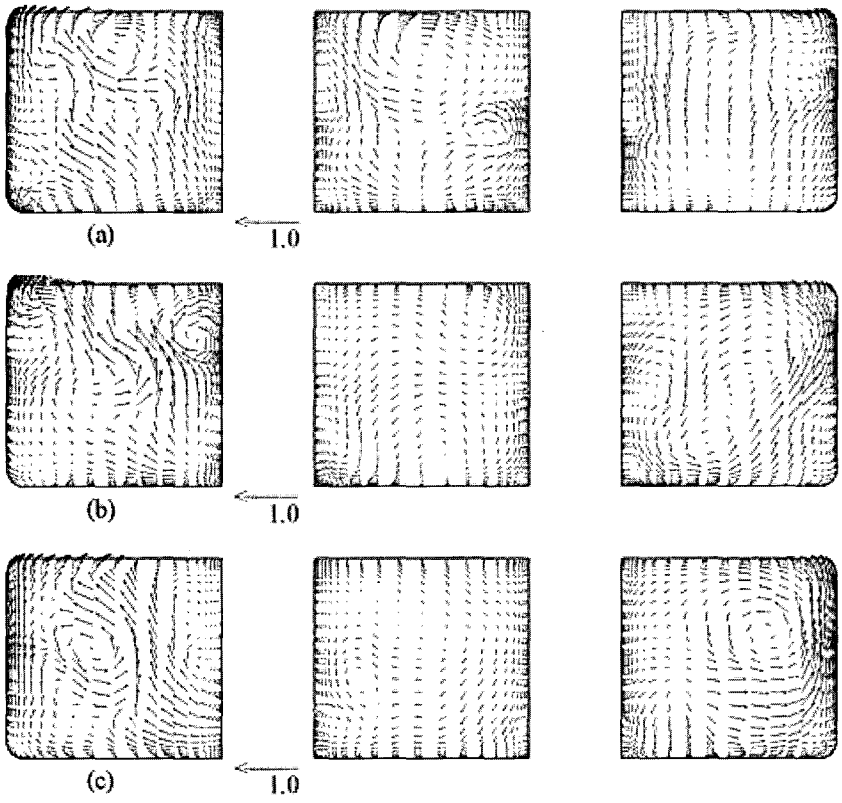

Fig. 10. Transverse velocity vectors at three locations downstream of the piers in the simulation of the draft tube.

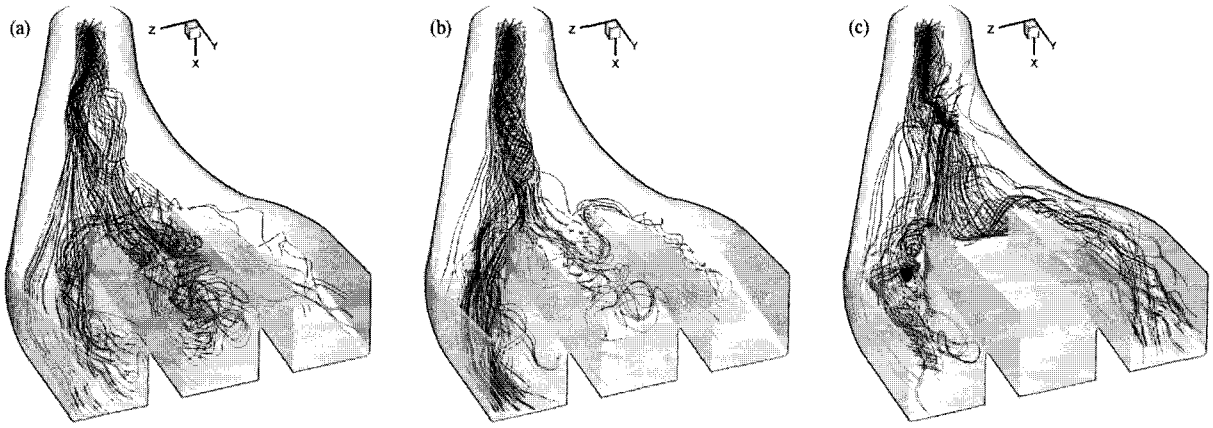

Fig. 11. Instantaneous particle paths at three instants in time in the simulation of the draft tube.

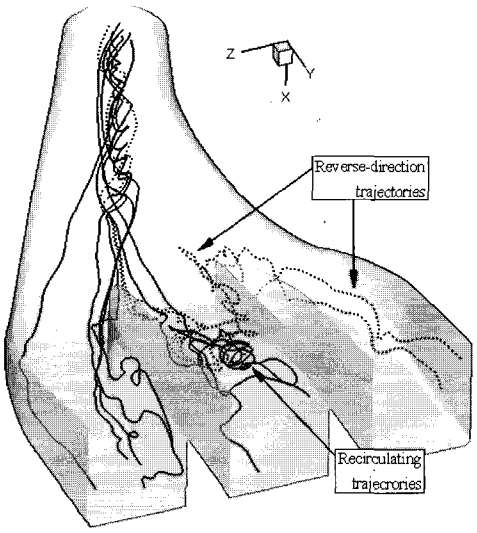

Fig. 12. Reverse-direction and recirculating particle trajectories in the simulation of the draft tube.

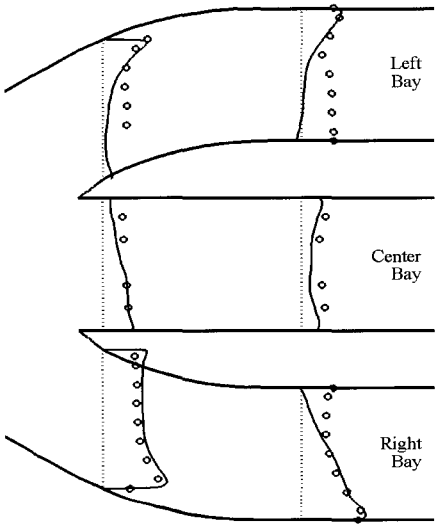

Fig. 13. Comparison of measured and computed axial mean velocity profiles along (a) the horizontal and (b) the vertical centerlines at two cross-sections located in the downstream diffuser: circle, experiments; Solid line, numerical solution.

Calculated time-average streamwise velocity profiles are compared with the experimental data (Hopping, 1992) in Figure 13, which shows profiles along the horizontal and vertical centrelines of each bay located at two stations in the downstream diffuser. The measurements in this figure suggest that most of the flow passes through the right bay, as mentioned, which is obviously associated with the counter-clockwise direction of the inflow swirl. The predictions of show this flow feature and appear to capture the general shape and magnitude of the measured profiles reasonably well. Some discrepancies are observed near the draft tube ceiling in the center and left bays and near the outside of both piers where the computed velocities are lower than measured. Theses discrepancies make also an interpretation that high velocity distribution near the junction of the bottom and the outside wall in the right bay is overestimated to some extent. It is important to emphasize, however, that the previously discussed assumption of axisymmetric flow at the inlet is likely to affect considerably the accuracy of the flow predictions in this region. Given the complexity of the geometry, the flow split among and distribution within the three bays could be very sensitive to even small asymmetries at the inlet.

Thus, without comprehensive measurements at the inlet to guide the specification of inflow conditions it is unlikely that better agreement between simulations and experiments can be achieved.

5. Conclusions

This paper presents numerical works carried out for developing an advanced computational framework for understanding injury- and mortality-inducing flow phenomena in hydropower plants. Large eddy simulation was used to predict the turbulent flow in a circular jet. Particle tracking studies with steady and unsteady versions of the rigid-virtual-fish model show that the flow environment experienced by a fish is drastically different when the forcing is provided by the true instantaneous flow rather than its statistically steady (statistical) mean representation. Fish passing through hydropower facilities interact and get injured by the instantaneous flow.

In this study a multi-domain CFD code is also developed that is capable of predicting the turbulent flow in real-life draft tubes using the DES technique. DESresults clearly show that the potential for disorientation and excessive residence times of fish within the draft tube is certainly considerable. Only unsteady calculations of the type reported here are capable of reproducing these effects and shedding light into their possible impact on passing fish. Current experience with the DES technique suggests that predicting the flow through the entire hydropower installations for studies of fish passage are attainable given adequate computer resources, that is, computers with on the order of 100 processors and the computer code that can take advantage of these processors in an efficient way.

The ultimate objective of the modeling work is to release the flexible virtual fishinto the simulated turbulent flow fields to be able to statistically characterize, for the first time, fish passage through the entire hydropower facility. With input from fish biologists, such statistical characterization of fish passage could lead to the firstrigorous framework for quantifying the fish friendliness of a given hydropower installation and for evaluating novel design concepts aimed at improving the compatibility of a hydropower plant with the aquatic habitat. For undertaking to be successful, however, modeling efforts must be supplemented by detailed field and laboratory flow experiments as well as experiments with live fish. Moreover, a close synergy between CFD modelers, hydraulic engineers, hydropower-plant operators, turbine designers, and fish biologists is also required.

Acknowledgments

The author is grateful to Fotis Sotiropolous for many useful discussionsand suggestions.

References

Abernethy, C.S., Amidan, B.G. and Čada. G.F. (2001). *Laboratory studies of the effects of pressure and dissolved gas supersaturation on turbine-passed fish.* DOE/ID-10853. U.S. Department of Energy Idaho Operations Office, Idaho Falls, Idaho.

Coutant, C.C., and Whitney, R.R. (2000). "Fish behavior in relation to passage through hydropower turbines: a review." *Transactions of the American Fisheries Society.* 129:351-380.

Grinstein, F. F., and DeVore, C.R. (1996). "Dynamics of coherent structures and transition to turbulence in free square jets." *Physics of Fluids*, Vol. 8, No. 5 pp. 1237-1251.

Hopping, P. N. (1992). *Draft tube measurements of water velocity and air concentration in the 1:11.71 scale model of the hydroturbines for Norris dam.* Report No. WR28-2-2-116, Tennessee Valley Authority Engineering Laboratory, Norris, Tennessee.

Nietzel, D.A., Richmond, M.C., Dauble, D.D., Mueller, R.P., Moursund, R.A., Abernethy, C.S., Guensch, G.R., and Čada, G.F. (2000). *Laboratory studies of the effects of shear on fish: final report.* DOE/ID-10822. U.S. Department of Energy Idaho Operations Office, Idaho Falls, Idaho.

Paik, J., Ge, L., and Sotiropolous, F. (2004). "Toward the simulation of complex 3D shear flows using unsteady statistical turbulence models." *International Journal of Heat and Fluid Flow.* Vol. 25,

No. 3, pp. 513-527.

Paik, J., Sotiropolous, F., and Sale, M.J. (2005). "Numerical simulation of swirling flow in a hydroturbine draft tube using unsteady statistical turbulence models." *Journal of hydraulic Engineering*, ASCE, In press.

Smagorinsky, J.S. (1963). "General circulation experiments with the primitive equations, part 1, basic experiments." *Mon, Weather Rev.* Vol. 91, pp. 99-164.

Shur, M., Spalart, P.R., Strelets, M., and Travin, A. (1999). "Detached-eddy simulation of an airfoil at high angle of attack." In: Rodi, W., Laurence, D. (Eds.), *Turbulent Shear Flows.*, Elsevier Science, Amsterdam, pp. 669 - 678.

Sotiropoulos, F., and Adballah, S. (2000). "A primitive variable method for the solution of 3D, incompressible, viscous flows." *Journal of computational Physics*, Vol. 103, pp. 339-349.

Sotiropoulos, F., and Constantinescu, G. (1997). "Pressure-based residual smoothing operators for multi-stage pseudo compressibility algorithms." *Journal of computational Physics*, Vol. 133, pp. 129-145.

Sotiropoulos, F., and Ventikos, Y. (1997). "The virtual fish concept: numerical prediction of fish passage through hydraulic power plants." *Proceedings of the 26th International Association of Hydraulic Research Congress.*

Spalart, P.R. (2000). "Strategies for turbulence modelling and simulations." *International Journal of Heat and Fluid Flow.* Vol. 21 pp. 252-263.

Spalart, P.R., and Allmaras, S.R. (1994). "A one-equation turbulence model for aerodynamic flows." *La Recherche Aerospatiale*, Vol. 1, pp. 5 - 21.

Spalart, P.R., Jou, W.H., Strelets, M., and Allmaras, S.R. (1997). "Comments on the feasibility of LES for wings and on a hybrid RANS/LES approach." In: Liu, C., Liu, Z. (Eds.), *Advances in DNS/LES, Greyden Press*, Columbus OH.

Squires, K.D., Forsythe, J.R., Morton, S.A., Strang, W.Z., Wurtzler, K.W., Tomaro, R.F., Grismer, M.J., and Spalart, P.R. (2002). "Progress on Detached-Eddy Simulation of massively separated flows." *AIAA Paper 2002-1021.*

Ventikos, Y., Sotiropoulos, F., and Patel, V.C. (1996). "Modelling complex draft-tube flows using near-wall turbulence closures." Pages 140-149 in E. Cabrera, V. Espert, and F. Martinez, eds. *Proceedings of 18th International Association of Hydraulic Research Symposium on Hydraulic Machinery and Cavitation*, Kluwer Academic Publishers, Boston.

Wilson, R.V., and Demuren, A.O. (1998). "Numerical simulation of turbulent jets with rectangular cross-section." *Journal of Fluids Engineering*, ASME, Vol. 120, pp. 285-290.

(논문번호:05-01/접수:2005.01.08/심사완료:2005.04.29)